

# Necklace-like states and persistent flows in spin-orbit-coupled Bose–Einstein condensates

Angela C. White,<sup>1</sup> Yongping Zhang,<sup>2,1,\*</sup> and Thomas Busch<sup>1</sup>

<sup>1</sup>*Quantum Systems Unit, Okinawa Institute of Science and Technology Graduate University, Onna, Okinawa 904-0495, Japan*

<sup>2</sup>*Department of Physics, Shanghai University, Shanghai 200444, China*

Necklace-like states, where periodically modulated densities bend into a ring shape, are well-known for their elegant appearance and the remarkable fact that they exist at all. However, they are often prone to different instabilities, which makes studying them rather difficult. Here we show that a Rashba spin-orbit-coupled Bose-Einstein condensate confined in a toroidal trap can provide a realistic experimental platform to create stable necklace-like states. We show that the number of petals composing the necklace-like state is highly tuneable and a function of the spin-orbit coupling strength, allowing a wide range of states to be created. In addition to necklace-like states, we show that the system also possesses states with persistent flow. We apply a simple but effective model to explain all features of the necklace-like states and the persistent flow states.

Necklace-like states, which are defined by their ring geometry and azimuthally periodic density modulation, are of great interest due to their unique way of breaking a system's symmetry. They were first theoretically proposed by Soljačić, Sears and Segev in a two dimensional homogenous nonlinear optical system [1, 2], and were later observed experimentally [3]. In homogenous systems however, necklace-like states are only quasi-stable and expand dynamically while keeping a necklace configuration. Stabilizing necklace-like states or slowing down the speed at which they expand are therefore interesting issues to address. In recent years, necklace-like states have been investigated in diverse physical situations, ranging from their creation via instabilities of ring dark solitons [4] and as vector solutions to the cubic non-linear Schrödinger equation [5, 6], to their appearance in situations where more complex non-linearities exist. The later include examples where non-linearities of different order compete [7–10], nonlocal nonlinearities exist [11–14] and where non-linearities are spatially modulated [15]. So far, a stationary necklace-like state has only been experimentally observed in a nonlinear optical system in the presence of an optically induced periodic potential that provides a mechanism to deeply trap each petal of the necklace into a corresponding cell of the potential. However, the number of petals is not adjustable and is limited to eight in the experiment [16].

In this work we show that stable necklace-like states can exist in two-dimensional toroidally trapped Bose-Einstein condensates (BEC) in the presence of Rashba-type spin-orbit coupling. We investigate the ground state phase diagram as a function of the spin-orbit coupling strength and find that in the immiscible regime, the two components each form a necklace-like state with the number of petals depending linearly on the spin-orbit coupling strength. In the miscible regime, both components form super-flows with different topological winding numbers. These winding numbers depend on the spin-orbit coupling strength and in all cases a unit winding num-

ber difference exists between the two components. All of these features originate from the spin-orbit coupling and can be physically understood via an effective one-dimensional azimuthal model.

Toroidal trapping potentials for atomic Bose-Einstein condensates allow for non-trivial geometries and have recently been created in several experiments. Different techniques exist, which include superposing a central repulsive potential barrier onto a harmonic trap [17] or intersecting a red-detuned sheet laser and a laser using a ring-shaped Laguerre-Gaussian mode [18, 19]. Rashba-type spin-orbit coupling has also been realised very recently in cold atomic gases [20, 21]. Our work, which describes the physics originating from applying Rashba spin-orbit coupling to BECs trapped in ring geometries, is therefore experimentally realistic and highly timely.

An atomic Bose-Einstein condensate with Rashba spin-orbit coupling can be described by the mean-field equations for the spinor wave function  $\Phi = (\Phi_1, \Phi_2)^T$  as

$$i\hbar \frac{\partial \Phi}{\partial t} = H\Phi + \Gamma\Phi, \quad (1)$$

where the single particle Hamiltonian is given by

$$H = \frac{p_x^2 + p_y^2}{2m_B} + V(x, y) + \lambda(p_y\sigma_x - p_x\sigma_y), \quad (2)$$

and the nonlinear part can be written as  $\Gamma = \text{diag}(g_{11}|\Phi_1|^2 + g_{12}|\Phi_2|^2, g_{12}|\Phi_1|^2 + g_{22}|\Phi_2|^2)$ . The toroidal trapping potential can be described by a shifted harmonic oscillator,  $V(x, y) = \frac{1}{2}m_B\omega_r^2(r - r_0)^2$ , where  $r^2 = x^2 + y^2$ . The toroidal radius is given by  $r_0$ , the harmonic trapping frequency by  $\omega_r$ , and  $m_B$  is the mass of the constituent bosons. The Rashba spin-orbit coupling strength is represented by  $\lambda$ , and the nonlinear mean-field coefficients  $g_{11}$  and  $g_{22}$  describe the s-wave scattering between atoms within each component, while  $g_{12}$  represents interactions between the two components. For simplicity, we assume that  $g_{11} = g_{22} = g$  and only consider  $\lambda > 0$ . Since the mean-field equations have a spin rotation symmetry, i.e.,  $U = \exp(i\pi\sigma_z/2)$ , the physics in the  $\lambda < 0$

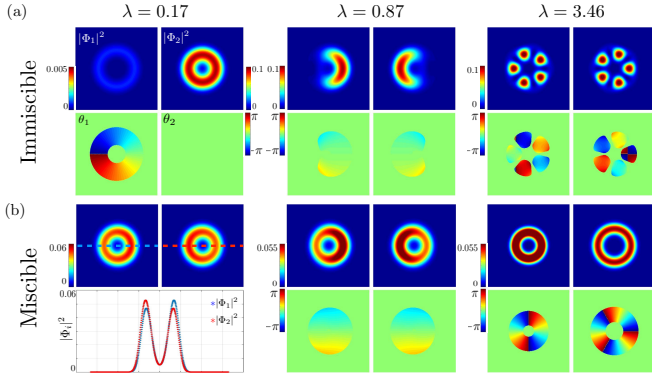


FIG. 1. (Color online) Row (a) depicts ground states of toroidally trapped condensates in the immiscible regime for  $g_{12}/g = 1.2$  with increasing spin-orbit coupling strength ( $\lambda = 0.17, 0.87$  and  $3.46$ ) and the top and bottom rows show density and phase profiles respectively. Row (b) shows the miscible regime ground-states for  $g_{12}/g = 0.4$ . The corresponding phase profiles are shown within the condensate edge (defined as 10% of the maximum condensate density). For  $\lambda = 0.17$ , the density profile for a slice through the centre of the condensate is shown below the full 2D density profiles (top row of b)). Here  $r_0 = 0.83$ .

regime is exactly same as that in the parameter regime of  $\lambda > 0$ .

In the following we will first numerically solve the above Hamiltonian, using standard imaginary time evolution, and then present an analytical model that confirms and explains our main numerical findings. In the numerical solutions the energy will be scaled in units of  $\hbar\omega_r$ , length in units of  $\sqrt{\hbar/m_B\omega_r}$  and  $\lambda$  in units of  $\sqrt{\hbar\omega_r/m_B}$ . Typical ground states in the immiscible and miscible regimes for small and large values of the spin-orbit coupling are shown in Fig. 1(a) and a number of interesting properties are immediately visible. In the immiscible regime, i.e. for  $g_{12}/g > 1$ , the two components spatially separate in order to minimize the mean-field energy, which is well known from the situations without spin-orbit coupling. In the absence of spin-orbit coupling, immiscible condensates phase separate radially in wide ring traps [22, 23], or azimuthally in narrow ring traps [22–25]. Phase separation is driven by trying to minimise the overall length of the domain boundaries, which usually leads to each component being concentrated in a single connected region. When spin-orbit coupling is introduced, however, each of the components breaks up into several parts along the azimuthal direction [26]. These parts form the petals of a necklace-like state, see Fig. 1(a) for  $\lambda = 3.46$ . For fixed trapping geometry and nonlinear coefficients, the number of petals,  $N_p$ , which is the same in each component, can be seen in Fig. 2(a) to follow an effectively linear dependence on the spin-orbit coupling strength  $\lambda$ . This provides a controllable method to create necklace-like states with an arbitrary number of petals. However, we note that an

odd number of petals composing the necklace-like states is dominant, which is apparent in both Figs. 1(a) and 2(a). We show below that only in very narrow regimes around certain discretised values of  $\lambda$  even-valued numbers of petals can be supported.

Ground states in the miscible regime, i.e. for  $g_{12}/g < 1$ , are shown in Fig. 1(b). Even though we intuitively expect no phase separation between the two components, it is intriguing to note that for smaller spin-orbit coupling strengths, the ground state can be seen to be slightly phase-separated even far away from the phase transition region. When the spin-orbit coupling strength is small, the bulk densities of each of the two components already occupy opposite sides of the ring (see  $\lambda = 0.17$  and  $\lambda = 0.87$  in Fig. 1(b)) and they become increasingly more phase-separated as  $g_{12}/g$  approaches unity. For larger values of  $\lambda$ , however, both components exhibit homogeneous density distributions around the ring (see  $\lambda = 3.46$  in Fig. 1(b)). From the phase profiles of these ground states, one can see that the winding numbers of each component can be nonzero and that there always exists a winding number difference of one unit between them. This difference in circulation results in unequal sizes of the ring-shaped densities, and the component with larger winding sits at a larger radius in the toroidal potential due to the centrifugal barrier. Such persistent flow is very different from that in toroidally trapped rotating two component Bose-Einstein condensates without spin-orbit coupling, where the two components carry the same winding number and always exhibit homogeneous density distributions in the miscible regime. This unit difference in winding number is maintained over a large range of values of  $\lambda$  (see Fig. 2(b)) and the numerically obtained ground-states indicate that the winding number of both components increases almost linearly as a function of  $\lambda$ .

The exotic properties of the ground state phase diagrams identified above are unique features arising from the presence of the Rashba spin-orbit coupling. To further understand the appearance of the necklace-like states with an odd number of petals across a broad range of spin-orbit coupling strengths in the immiscible regime, and the weak phase separation and persistent flows with a unit winding number difference in the miscible regime, we will in the following use an effective one-dimensional model to provide a physical picture.

Since all of the effects highlighted above are along the azimuthal direction, we will in the following assume that the harmonic trap frequency  $\omega_r$  is very large, so that the dynamics along the radial direction are completely confined to the lowest mode of the harmonic trap. This allows us to use an effective one-dimensional model, retaining only the degree of freedom along the azimuthal direction and integrating out any dynamics in the radial direction. For this we make the approximation  $\Phi = R(r)\Phi(\phi)$ , where  $R(r)$  is just the ground state in the harmonic po-

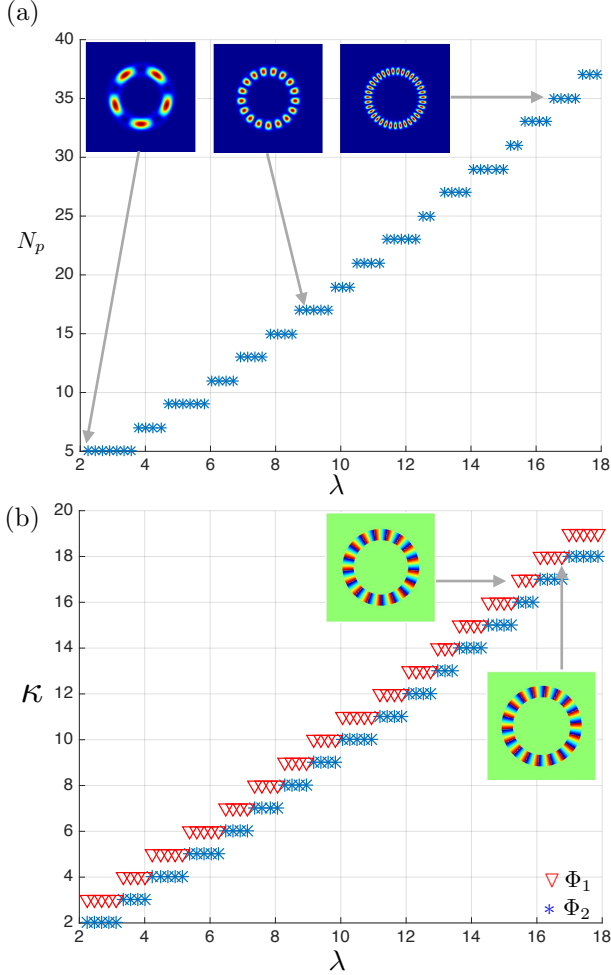


FIG. 2. (Color online) (a) Number of petals as a function of the spin-orbit coupling strength in the immiscible regime  $g_{12}/g = 1.6$ . The insets show the density profiles of a single component, confirming the typical necklace-like appearance over a large range of values of  $\lambda$ . (b) Winding numbers of  $\Phi_1$  and  $\Phi_2$  as a function of the spin-orbit coupling strength  $\lambda$  in the miscible regime ( $g_{12}/g = 0.6$ ). The insets show the phase profile for  $\lambda = 16.8$ . Here  $r_0 = 1.12$ .

tential in the radial direction,  $r$ . The total energy is then given by

$$E_{\text{tot}} = \frac{1}{2\pi} \int_0^{2\pi} d\phi \left[ \bar{\Phi}^* H_{\text{eff}} \bar{\Phi} + \frac{\bar{g}}{2} |\bar{\Phi}_1|^4 + \frac{\bar{g}}{2} |\bar{\Phi}_2|^4 + \bar{g}_{12} |\bar{\Phi}_1|^2 |\bar{\Phi}_2|^2 \right], \quad (3)$$

where  $\phi$  is the azimuthal angle. The azimuthal single-particle Hamiltonian,  $H_{\text{eff}}$ , is given by [27, 28]

$$H_{\text{eff}} = \left( -i \frac{\partial}{\partial \phi} \right)^2 + \bar{\lambda} (\cos(\phi) \sigma_x + \sin(\phi) \sigma_y) \left( -i \frac{\partial}{\partial \phi} + \frac{\sigma_z}{2} \right), \quad (4)$$

where the energy and time units are  $\hbar^2/2m_B r_0^2$  and  $2m_B r_0^2/\hbar$ , respectively. Other parameters are scaled as  $\bar{\lambda} = 2m_B r_0 \lambda/\hbar$  and  $\bar{g}_{ij} = \sqrt{2m_B^3/\pi \hbar^5} r_0 g_{ij}$ . The single-particle Hamiltonian  $H_{\text{eff}}$  is invariant under a rotation

$U = \exp(i\varphi J_z)$  due to the conservation of  $J_z$ , where  $\varphi$  is an arbitrary angle and  $J_z = -i\partial/\partial\phi + \sigma_z/2$  [29]. This rotation invariance requires that a general ansatz to solve  $H_{\text{eff}}$  should have the form

$$\bar{\Phi}_s(m) = \exp(im\phi) \begin{pmatrix} \bar{\Phi}_1 \\ \exp(i\phi) \bar{\Phi}_2 \end{pmatrix}, \quad (5)$$

where the integer number  $m$  characterizes the phase winding induced by the spin-orbit coupling and there is always a unit winding number difference between the components. The eigenvalues of  $H_{\text{eff}}$  can be analytically found as

$$E_{\pm}(m) = \frac{m^2 + (1+m)^2}{2} \pm |m + \frac{1}{2}| \sqrt{\bar{\lambda}^2 + 1} \quad (6)$$

and it is straightforward to see that the lower branch satisfies the degeneracy  $E_-(m) = E_-(-m-1)$ . If  $\sqrt{\bar{\lambda}^2 + 1}/2$  is not an integer, the minima of  $E_-$  appear for  $m^*$  and  $-m^* - 1$ , where  $m^*$  is an integer in the regime  $\frac{\sqrt{\bar{\lambda}^2 + 1}}{2} - 1 < m^* < \frac{\sqrt{\bar{\lambda}^2 + 1}}{2}$ . The lowest single particle state is therefore two-fold degenerate. However, when  $\sqrt{\bar{\lambda}^2 + 1}/2$  is an integer, the minima of  $E_-$  appear for  $m^*$ ,  $m^* - 1$ ,  $-m^* - 1$  and  $-m^*$ , with  $m^*$  being  $m^* = \frac{\sqrt{\bar{\lambda}^2 + 1}}{2}$ . The lowest single particle state is then four-fold degenerate.

Based on these single-particles wave functions, we can now construct the ground state in the presence of the mean-field interactions. In the case of two-fold degeneracy, the trial ground state wave function is a superposition of the wave functions at the minima located at  $m^*$  and  $-m^* - 1$  and can be written as [30, 31]

$$\bar{\Phi} = C_1 \exp(im^* \phi) \begin{pmatrix} \cos \theta \\ -\exp(i\phi) \sin \theta \end{pmatrix} + C_2 \exp(-im^* \phi) \begin{pmatrix} \exp(-i\phi) \sin \theta \\ \cos \theta \end{pmatrix}, \quad (7)$$

where  $2\theta = \arctan(\bar{\lambda})$  with  $(0 < \theta < \pi/2)$ , which relates to the single-particle wave function at the minima. The coefficients  $C_1$  and  $C_2$  satisfy  $|C_1|^2 + |C_2|^2 = 1$  and can be determined by minimizing the total energy of the Hamiltonian in Eq. (3). Substituting the trial wave function into this expression we therefore obtain

$$E_{\text{tot}} = \frac{2 - \bar{\lambda}^2}{2(1 + \bar{\lambda}^2)} (g_{12} - g) |C_1|^2 |C_2|^2 + E_{\text{con}}, \quad (8)$$

where  $E_{\text{con}} = \bar{\lambda}^2(g_{12} - g)/4(1 + \bar{\lambda}^2) + g/2 + m^{*2} + (m^* + 1/2)(1 + \sqrt{1 + \bar{\lambda}^2})$ . Minimizing  $E_{\text{tot}}$  with respect to  $|C_1|^2 |C_2|^2$  then leads to the following situations.

(1) For the immiscible case ( $g_{12} > g$ ) and in the parameter regime of  $\bar{\lambda} > \sqrt{2}$ , one finds  $|C_1|^2 = |C_2|^2 = 1/2$ . The density distributions of the ground state wave functions become  $|\bar{\Phi}_1|^2 = 1 + \frac{1}{2} \sin(2\theta) \cos[(2m^* + 1)\phi + \chi]$  and  $|\bar{\Phi}_2|^2 = 1 - \frac{1}{2} \sin(2\theta) \cos[(2m^* + 1)\phi + \chi]$ , where  $\chi$  is the

phase of  $C_1 C_2^*$ , which can not be fixed by the energy minimization. It is apparent that the two components feature spatial separation along the azimuthal direction,  $\phi$ , and possess equal periodicity of  $2\pi/(2m^* + 1)$ , indicating that there are  $2m^* + 1$  density blocks in each component. Combining this azimuthal solution with the ground state in the radial direction leads to the appearance of spatially separated necklace-like states, with odd numbers of petals in each component, confirming the observation in the numerical simulations (see Fig. 1(a) and Fig. 2(a)). The state in Eq. (7) with  $|C_1|^2 = |C_2|^2 = 1/2$  is analogous to the so-called stripe phase, known to occur in harmonically trapped or homogenous spin-orbit coupled condensates [32, 33].

(2) In the parameter regime of  $0 < \bar{\lambda} < \sqrt{2}$  in the immiscible case, the energy minimization requires  $|C_1|^2 |C_2|^2 = 0$ , resulting in two possible states,  $C_1 = 1$  and  $C_2 = 0$ , or  $C_1 = 0$  and  $C_2 = 1$ , with density distributions  $|\bar{\Phi}_1|^2 = \cos^2(\theta)$  and  $|\bar{\Phi}_2|^2 = \sin^2(\theta)$  or  $|\bar{\Phi}_1|^2 = \sin^2(\theta)$  and  $|\bar{\Phi}_2|^2 = \cos^2(\theta)$ , respectively. These states are spatially homogenous along  $\phi$ , and one of the two components dominates and is composed of the majority of atoms, as  $\cos^2(\theta) = \frac{1}{2}(1 + \frac{1}{\sqrt{1+\bar{\lambda}^2}})$ . This is evident in Fig. 1(a), for a spin-orbit coupling strength of  $\lambda = 0.17$ . Since  $0 < \bar{\lambda} < \sqrt{2}$ ,  $m^*$  is fixed to  $m^* = 0$ , which indicates that only one component has phase winding. The existence of these spatially homogenous states seems to be counter-intuitive in the immiscible regime, where phase separation is expected. However, the large imbalance in the number of atoms in each component and the presence of a difference in phase winding between the two components makes these states energetically preferable.

(3) For the miscible case ( $g_{12} < g$ ) and in the regime where  $\bar{\lambda} > \sqrt{2}$ , the minimization of the total energy leads to  $|C_1|^2 |C_2|^2 = 0$ . Similar to the situation considered in (2), the ground states consist of homogenous states with phase winding, i.e., one component has a winding number  $m^*$  and the other has winding of  $m^* + 1$ , or one component has winding  $-m^* - 1$  while the other has  $-m^*$ . Note that there is always a unit winding number difference between two components. Since  $\frac{\sqrt{\bar{\lambda}^2+1}}{2} - 1 < m^* < \frac{\sqrt{\bar{\lambda}^2+1}}{2}$ , the winding numbers increase roughly linearly as a function of the spin-orbit coupling strength  $\bar{\lambda}$  (see Fig. 2(b)). Due to phase winding, these states carry macroscopic flows without dissipation and we call them persistent flow states.

(4): When  $0 < \bar{\lambda} < \sqrt{2}$  in the miscible regime, energy minimisation leads to  $|C_1|^2 = |C_2|^2 = 1/2$  and one again can find states with a degree of phase separation, similar to those found in case (1). However, these are different to the phase separated states of necklace-like form in the immiscible regime. For the miscible states one has  $m^* = 0$  and therefore only one petal is expected. This behaviour coincides with the one observed in Fig. 1(b)

for  $\lambda = 0.17$  and  $0.87$ .

In the above calculations, we have used a variational method and applied a one-dimensional model to understand the features of the two-dimensional, numerical ground states. In particular, this approach explains the linear dependence of the number of petals on the spin-orbit coupling strength (as shown in Fig. 2(a)) and the appearance and behaviour of the winding numbers (as shown in Fig. 2(b)). Additionally, the variational ansatz confirms that the ground-states consist of an odd number of petals,  $2m^* + 1$ . This is due to the fact that only two modes,  $C_1$  and  $C_2$ , are assumed to play a role, since the lowest single-particle state is two-fold degenerate. However, if  $\frac{\sqrt{\bar{\lambda}^2+1}}{2}$  is an integer, the lowest single particle eigenstate is four-fold degenerate. In this case the ground state trial wave function should be chosen as a superposition of four modes,  $\bar{\Phi} = C_1 \Phi_{\sin}(m^*) + C_2 \Phi_{\sin}(-m^* - 1) + C_3 \Phi_{\sin}(m^* - 1) + C_4 \Phi_{\sin}(-m^*)$ , with  $m^* = \frac{\sqrt{\bar{\lambda}^2+1}}{2}$ , and such a trial wave function could result in an even number of petals. However, requiring that  $\frac{\sqrt{\bar{\lambda}^2+1}}{2}$  must be an integer means that only very close to certain discretised spin-orbit coupling strengths necklace-like states composed of an even number of petals can be expected, which explains why in the numerical simulations shown in Fig. 2(a) only states with odd numbers of petals are visible.

In conclusion, we have shown that Rashba spin-orbit-coupled Bose-Einstein condensates in a toroidal geometry can serve as a flexible platform to realise stable necklace-like states. We have systematically investigated the exotic ground state properties of such a system. In addition to necklace-like states, the ground states may support persistent flow. An effective one-dimensional azimuthal model was explored, and the application of a variational method was found to provide a quantitative understanding of all the salient features of the different ground state phases in the miscible and immiscible regimes. The necklace-like states as well as states with persistent flow originate from Rashba-type spin-orbit-coupling which is two-dimensional, and they cannot exist for one-dimensional spin-orbit coupling in a ring trap [34].

Acknowledgements: This work was supported by the Okinawa Institute of Science and Technology Graduate University. Angela C. White and Thomas Busch were supported by JSPS KAKENHI-16K05461. Yongping Zhang is supported in part by the Thousand Young Talent Program of China, and Eastern Scholar Program of Shanghai.

---

\* [yongping11@t.shu.edu.cn](mailto:yongping11@t.shu.edu.cn)

[1] M. Soljačić, S. Sears, and M. Segev, Phys. Rev. Lett. **81**,

- 4851 (1998). Self-trapping of “necklace” beams in self-focusing Kerr media.
- [2] M. Soljačić and M. Segev, *Phys. Rev. Lett.* **86**, 420 (2001). Integer and fractional angular momentum borne on self-trapped necklace-ring beams.
  - [3] T.D. Grow, A.A. Ishaaya, L.T. Vuong, and A.L. Gaeta, *Phys. Rev. Lett.* **99**, 133902 (2007). Collapse and stability of necklace beams in Kerr media.
  - [4] G. Theocharis, D.J. Frantzeskakis, P.G. Kevrekidis, B.A. Malomed, and Y.S. Kivshar, *Phys. Rev. Lett.* **90**, 120403 (2003). Ring dark solitons and vortex necklaces in Bose-Einstein condensates.
  - [5] A.S. Desyatnikov and Y.S. Kivshar, *Phys. Rev. Lett.* **87**, 033901 (2001). Necklace-ring vector solitons.
  - [6] V.M. Lashkin, E.A. Ostrovskaya, A.S. Desyatnikov, and Y.S. Kivshar, *Phys. Rev. A* **80**, 013615 (2009). Vector azimuthons in two-component Bose-Einstein condensates.
  - [7] Y.V. Kartashov, L.-C. Crasovan, D. Mihalache, and L. Torner, *Phys. Rev. Lett.* **89**, 273902 (2002). Robust propagation of two-color soliton clusters supported by competing nonlinearities.
  - [8] D. Mihalache, D. Mazilu, L.-C. Crasovan, B.A. Malomed, F. Lederer, and L. Torner, *Phys. Rev. E* **68**, 046612 (2003). Robust soliton clusters in media with competing cubic and quintic nonlinearities.
  - [9] L. Dong, J. Wang, H. Wang, and G. Yin, *Phys. Rev. A* **79**, 013807 (2009). Bessel lattice solitons in competing cubic-quintic nonlinear media.
  - [10] Y. He, D. Mihalache, B.A. Malomed, Y. Qiu, Z. Chen, and Y. Li, *Phys. Rev. E* **85**, 066206 (2012). Generation of polygonal soliton clusters and fundamental solitons in dissipative systems by necklace-ring beams with radial-azimuthal phase modulation.
  - [11] C. Rotschild, M. Segev, Z. Xu, Y.V. Kartashov, L. Torner, and O. Cohen, *Opt. Lett.* **31**, 3312 (2006). Two-dimensional multipole solitons in nonlocal nonlinear media.
  - [12] D. Buccoliero, A.S. Desyatnikov, W. Krolikowski, and Y.S. Kivshar, *Phys. Rev. Lett.* **98**, 053901 (2007). Laguerre and Hermite soliton clusters in nonlocal nonlinear media.
  - [13] W.-P. Zhong and M. Belić, *Phys. Rev. A* **79**, 023804 (2009). Three-dimensional optical vortex and necklace solitons in highly nonlocal nonlinear media.
  - [14] M. Shen, Q. Kong, C.-C. Jeng, L.-J. Ge, R.-K. Lee, and W. Krolikowski, *Phys. Rev. A* **83**, 023825 (2011). Instability suppression of clusters of vector-necklace-ring solitons in nonlocal media.
  - [15] Y.V. Kartashov, B.A. Malomed, V.A. Vysloukh, and L. Torner, *Phys. Rev. A* **80**, 053816 (2009). Stabilization of multi-beam necklace solitons in circular arrays with spatially modulated nonlinearity.
  - [16] J. Yang, I. Makasyuk, P.G. Kevrekidis, H. Martin, B.A. Malomed, D.J. Frantzeskakis, and Z. Chen, *Phys. Rev. Lett.* **94**, 113902 (2005). Necklcelike solitons in optically induced photonic lattices.
  - [17] C. Ryu, M.F. Andersen, P. Cladé, V. Natarajan, K. Helmerson, and W.D. Phillips, *Phys. Rev. Lett.* **99**, 260401 (2007). Observation of persistent flow of a Bose-Einstein condensate in a toroidal trap.
  - [18] A. Ramanathan, K.C. Wright, S.R. Muniz, M. Zelan, W.T. Hill III, C.J. Lobb, K. Helmerson, W.D. Phillips, and G.K. Campbell, *Phys. Rev. Lett.* **106**, 130401 (2011). Superflow in a toroidal Bose-Einstein condensate: an atom circuit with a tunable weak link.
  - [19] S. Beattie, S. Moulder, R.J. Fletcher, and Z. Hadzibabic, *Phys. Rev. Lett.* **110**, 025301 (2013). Persistent currents in spinor condensates.
  - [20] L. Huang, Z. Meng, P. Wang, P. Peng, S.-L. Zhang, L. Chen, D. Li, Q. Zhou, and J. Zhang, *Nature Physics* **12**, 540 (2016). Experimental realization of a two-dimensional synthetic spin-orbit coupling in ultracold Fermi gases.
  - [21] Z. Wu, L. Zhang, W. Sun, X.-T. Xu, B.-Z. Wang, S.-C. Ji, Y. Deng, S. Chen, X.-J. Liu, and J.-W. Pan, *Science* **354**, 83 (2016). Realization of two-dimensional spin-orbit coupling for Bose-Einstein condensates.
  - [22] P. Mason, *Eur. Phys. J. B* **86**, 453 (2013). Ground states of two-component condensates in a harmonic plus Gaussian trap.
  - [23] M. Abad, A. Sartori, S. Finazzi, and A. Recati, *Phys. Rev. A* **89**, 053602 (2014). Persistent currents in two-component condensates in a toroidal trap.
  - [24] T. Shimodaira, T. Kishimoto, and H. Saito, *Phys. Rev. A* **82**, 013647 (2010). Connection between rotation and miscibility in a two-component Bose-Einstein condensate.
  - [25] A. White, T. Hennessy, and Th. Busch, *Phys. Rev. A* **93**, 033601 (2016). Emergence of Classical Rotation in Superfluid Bose-Einstein Condensates.
  - [26] Xiao-Fei Zhang, Masaya Kato, Wei Han, Shou-Gang Zhang, Hiroki Saito, *ArXiv:1610.09458*. Spin-orbit-coupled Bose-Einstein condensates held under toroidal trap.
  - [27] O. Fialko, J. Brand, and U. Zülicke, *Phys. Rev. A* **85**, 051605(R) (2012). Soliton magnetization dynamics in spin-orbit-coupled Bose-Einstein condensates
  - [28] F.E. Meijer, A.F. Morpurgo, and T.M. Klapwijk, *Phys. Rev. B* **66**, 033107 (2002). One-dimensional ring in the presence of Rashba spin-orbit interaction: Derivation of the correct Hamiltonian.
  - [29] E. Ruokokoski, J. A. M. Huhtamäki, and M. Möttönen, *Phys. Rev. A* **86**, 051607(R)(2012). Stationary states of trapped spin-orbit-coupled Bose-Einstein condensates.
  - [30] Y. Li, L.P. Pitaevskii, and S. Stringari, *Phys. Rev. Lett.* **108**, 225301 (2012). Quantum tricriticality and phase transitions in spin-orbit coupled Bose-Einstein condensates.
  - [31] K. Sun, C. Qu, and C. Zhang, *Phys. Rev. A* **91**, 063627 (2015). Spin-orbital-angular-momentum coupling in Bose-Einstein condensates.
  - [32] Chunji Wang, Chao Gao, Chao-Ming Jian, and Hui Zhai, *Phys. Rev. Lett.* **105**, 160403 (2010). Spin-Orbit Coupled Spinor Bose-Einstein Condensates.
  - [33] T.-L. Ho, and S. Zhang, *Phys. Rev. Lett.* **107**, 150403 (2011). Bose-Einstein Condensates with Spin-Orbit Interaction.
  - [34] E. Ö. Karabulut, F. Malet, A. L. Fetter, G. M. Kavoulakis, and S. M. Reimann, *New Journal of Physics* **18**, 015013 (2016). Spin-orbit-coupled Bose-Einstein-condensed atoms confined in annular potentials.